Dendritic magnetite nanocarriers for drug delivery applications

Sudeshna Chandra, Shailee Mehta, Saumya Nigam and D. Bahadur*

Received (in Victoria, Australia) 28th October 2009, Accepted 19th December 2009
First published as an Advance Article on the web 12th February 2010
DOI: 10.1039/b9nj00609e

A novel arginine-based dendritic block is grown on the surface of APTS-coated Fe_3O_4 nanoparticles by conventional growth approach of Michael addition/amidation reactions. The thus-obtained dendritic magnetite nanocarriers (DMNCs) were characterized by X-ray diffraction (XRD), Fourier transform infrared spectroscopy (FTIR), transmission electron microscopy (TEM), atomic force microscopy (AFM), vibrating sample magnetometry(VSM), dynamic light scattering (DLS) and thermogravimetric (TGA) analysis. The functionalization of MNPs with the dendritic block was evident from FTIR and TGA analyses. The nanocarriers had an average size of 10 nm and exhibited superparamagnetism with high magnetization values at room temperature. The aqueous colloidal suspension of DMNCs (10 mg ml^{-1} of Fe) showed a temperature rise up to 43 °C in 5 min and yielded a moderate specific absorption rate (SAR) value of 30 W g^{-1} of magnetite under the influence of AC magnetic field of 10 kA m^{-1} and 425 kHz frequency. Biocompatibility of the developed nanocarriers was evaluated *in vitro* by assessing their cytotoxicity on human cervical cancer cells (HeLA cells) using a sulforhodamine B (SRB) assay. Encapsulation and release of the anticancer drug doxorubicin (DOX) was investigated. The change in surface charge, as evident from zeta potential analyzer and quenching of fluorescence intensity, strongly suggests the interaction of DOX with the DMNCs. The nanocarriers showed good capacity to encapsulate DOX, with loading as high as 65% (w/w) and a pH-responsive sustained release of 54% at pH 5.0. Also, the release of DOX from the nanocarriers increased up to 80% on application of an AC magnetic field.

1. Introduction

Superparamagnetic iron oxide nanoparticles have been extensively studied for various biological applications like drug delivery, magnetic resonance imaging, protein immobilization and many others.[1–5] Due to relatively large surface area, nanometer-sized superparamagnetic iron oxide particles have a strong tendency to agglomerate by van der Waals force and magnetic dipole–dipole interaction. So, it is necessary to develop new synthetic strategies to chemically stabilize these magnetic colloidal nanoparticles. For all mentioned applications, modification of the iron oxide surface is done through creation of layers of organic molecules, polymers, inorganic systems and macromolecules so as to functionalize their surfaces for attachment of bioactive molecules. This can be done either by embedding the iron oxide nanoparticles in matrices or by encapsulating the nanoparticles with macromolecules. Embedment of iron oxide nanoparticles in polymeric matrices can prevent agglomeration in physiological media; however, it is difficult to produce a high density of functional groups for conjugating with bio-molecules. Therefore, encapsulating the iron oxide nanoparticles by macromolecules is a better option since it not only prevents aggregation and preserves their physiochemical properties, but also provides multiple surface functionalities, which are very important for bio-applications.

Department of Metallurgical Engineering and Material Science, Indian Institute of Technology Bombay, Powai, Mumbai-400076, India. E-mail: dhirenb@iitb.ac.in; Fax: +91 22 2572 3480; Tel: +91 22 2576 7632

In this respect, dendritic macromolecules have an edge over other linear polymeric macromolecules since they not only provide functional groups but also have an internal cavity which can entrap a guest, for example, drug, target ligand, fluorescence moiety *etc*. Coupling the drug molecules directly to the dendritic surface or trapping the drug within the cavities of the dendritic macromolecule are the various ways to prepare macromolecule–drug conjugates. Because of its multiple surface functionalities, the dendritic–drug conjugate is able to carry drug molecules, and also the number of drug molecules per conjugate can be varied by using different monomers for obtaining the dendritic block. There are various strategies for entrapment of the guest molecules with the dendritic structure,[6] the first being reported by Jansen *et al*.,[7] based on physical encapsulation. Another strategy is based on multiple chemical interactions between guest molecules and the dendritic structure.[8,9] The third strategy involves micellar interaction between amphiphilic dendritic macromolecules and guest molecules which are capable of dissolving various hydrophobic compounds (drugs) in aqueous medium.[10,11] However, to develop an efficient drug delivery system, it is essential to consider some important factors, such as loading and transporting drugs, and the release of the drug to the desired site (cancer cells) within a given period of time (sustained release). Several research groups[12,13] have reported dendrimer-tailored drug delivery systems to release the active agents through varying the environmental factors such as pH and temperature. Currently, improvement in drug loading and release remains a major challenge in dendritic delivery systems.

To this end, very few efforts have been made to enhance the ability of the dendrimers to encapsulate drugs.[14,15] Further, application of dendrimers as a potential drug carrier requires focus on their biocompatibility. Currently, there are only a few commercially available dendrimers like poly(amidoamine) (PAMAM) and poly(propyleneimine) (PPI) dendrimers which are not biocompatible due to their polycationic character.[16–18] As a result, the search for new water-soluble and biocompatible dendritic systems for drug delivery purposes is of considerable interest.

Described within this paper is the direct formation of a dendritic block on the surface of aminosilane-modified magnetic nanoparticles (nanocarriers) for biological applications. The structure of the novel dendritic system was tailored by using methyl acrylate and biocompatible arginine as branching units. The developed nanocarriers have been investigated for possible drug delivery and hyperthermia treatment of cancer. The surface functionality of the nanocarriers can be used for further conjugation of various biomolecules.

2. Results and discussion

A dendritic structure was grown on the surface of Fe_3O_4-coated aminosilane particles employing a divergent route starting from the amine-functionalized iron oxide core. A Michael-type addition reaction took place between the pre-existing amino groups on iron oxide nanoparticles and the methyl acrylate with the ratio of two propionate ester groups to one amino group. Subsequent ester moieties reacted with arginine to achieve the dendritic macromolecule (Scheme 1). These processes were monitored with FTIR (Fig. 1).

In our work, the Fe_3O_4 nanoparticles were coated with aminosilane in order to make particles with high dispersion and biocompatibility.[19] The magnetic Fe_3O_4 nanoparticles (MNPs) were coated with 3-aminopropyl-trimethoxysilane (APTS) by chemical reaction between the –OH on the surface of the Fe_3O_4 and Si–OMe of APTS. The characteristic absorption

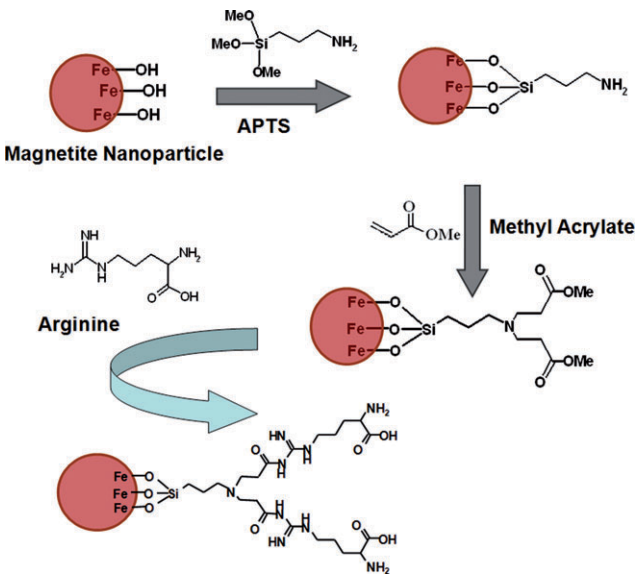

Scheme 1 Growth of the dendritic block on the magnetic nanoparticles.

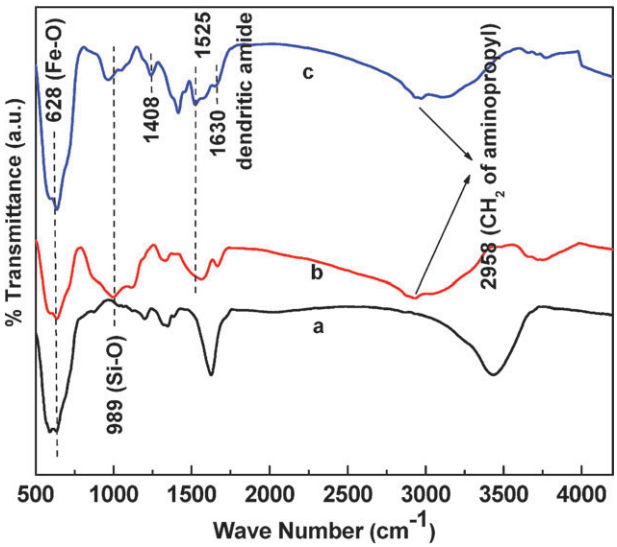

Fig. 1 FTIR spectra of (a) MNPs, (b) APTS-coated MNPs and (c) DMNCs.

band for the Fe–O bond of Fe_3O_4 nanoparticles appears at 628 and 585 cm^{-1} in all the samples (Fig. 1). FTIR of APTS-coated magnetic nanoparticles (APTS-coated MNPs) show absorptions at ~3500 and 1600 cm^{-1} which are due to O–H stretching and bending vibrations of physically adsorbed water and surface –OH groups, respectively. Bands at 3082 and 2958 cm^{-1} correspond to the $-CH_2$ group of the aminopropyl attached to the Si, and these are absent in bare iron oxide. The stretching vibrations of C–N and Si–O bands in APTS-coated MNPs are observed at 1117 and 989 cm^{-1} respectively. When compared to the FTIR of the DMNCs, the Si–O band at 989 cm^{-1} shifts slightly to a lower wavenumber. The absorption bands at 3285 cm^{-1} (due to the bending vibration of the $-NH_2$) and 2958 cm^{-1} (due to stretching of C–H bond) are indicative of the presence of the arginine monomer of the dendritic structure. The bands at ~1630, 1525 and 1408 cm^{-1}, due to the presence of the amide group, were also observed in the DMNCs, which are absent in APTS-coated MNPs and bare MNPs. This gives strong evidence of the modification of the APTS-coated MNPs. Measurement of the dendritic zeta potential of the APTS-coated MNPs as a function of pH was also performed to confirm the surface charge properties. The pH values of the suspension were adjusted in the range of 3–10. A positive zeta potential is observed due to the presence of the amino group ($-NH_2$) of APTS, which exists as $-NH_3^+$ in water by the attraction of protons to the negatively charged nitrogen atom. The zeta potentials decrease with pH values, especially at high pH range as depicted in Fig. 2.

Fig. 3 shows the XRD patterns of MNPs and dendritic magnetite nanocarriers (DMNCs). The XRD analysis reveals the formation of single-phase Fe_3O_4 in a cubic inverse-spinel structure. The crystallite size of MNPs and DMNCs were found to be 9.2 and 9.8 nm, respectively, from X-ray line broadening. The XRD pattern of DMNCs (inset of Fig. 3) clearly shows shifting of the center of diffraction lines towards lower angle in comparison to that of MNPs, which in turn indicate a slight increase in the lattice parameter of DMNCs.

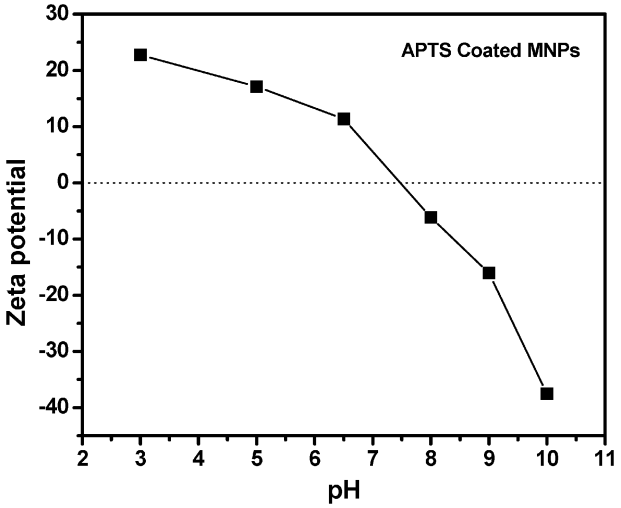

Fig. 2 pH-dependent zeta potential curve of APTS-coated MNPs.

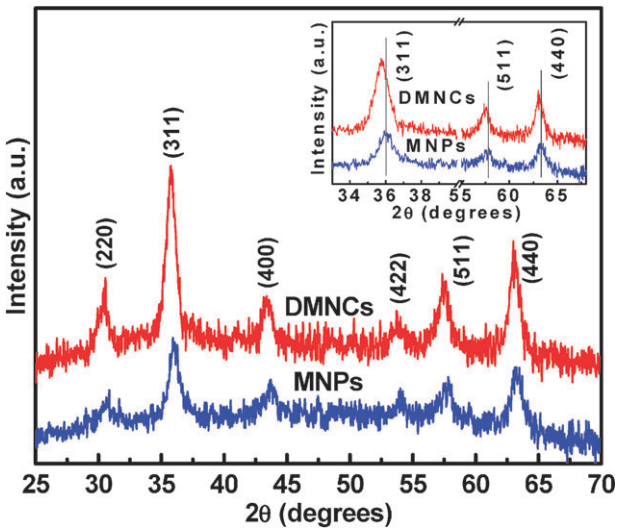

Fig. 3 XRD patterns of the MNPs and DMNCs. The inset shows the shifting of diffraction lines of (311), (511) and (440) planes of DMNCs towards lower angle.

Furthermore, an increase of about 0.5% was observed in the lattice parameter, whereas the change in lattice strain is found to be negligible from the XRD data. The surface atoms of the MNPs have broken (unsatisfied) bonds, which are pulled inward by the subsurface atomic layers, thereby lowering the bond length and the lattice parameter. Upon functionalization of MNP with dendritic block (DMNCs), the broken bonds of the surface atoms are reformed and hence the surface ions are readily repelled from the interior, leading to an increase in the lattice parameter.[20] This provides important supporting evidence of the functionalization of the MNPs with the dendritic moiety.

Weight loss of the dendritic magnetite nanocarriers (DMNCs) between 30 to 500 °C as a function of temperature was determined using TGA, which is an irreversible process because of the thermal decomposition. Fig. 4 shows TGA plots depicting two-step thermal decomposition of MNPs, APTS-coated MNPs and DMNCs. The first-step weight loss

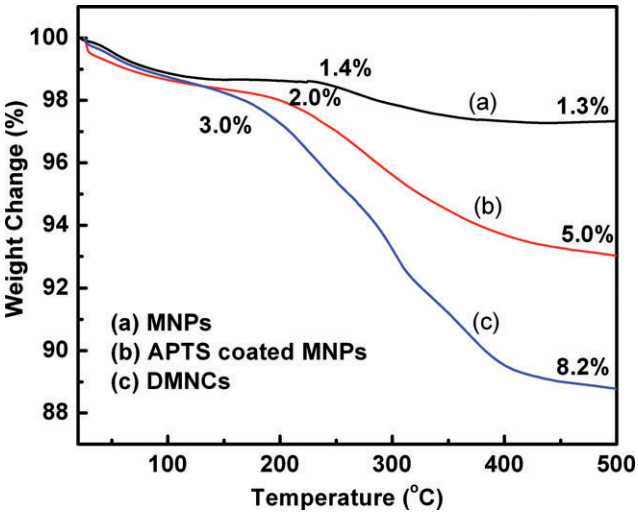

Fig. 4 TGA curves of MNPs, APTS-coated MNPs and DMNCs.

in case of MNPs corresponds to the removal of physically adsorbed water and –OH groups, whereas in the other two cases, the weight loss is also associated with the removal of physically adsorbed organic molecules along with the physically adsorbed water and –OH groups. The second-step weight loss in MNPs is possibly due to the structural transformation of Fe_3O_4. However, the greater weight loss in second-step thermal decomposition of APTS-coated MNPs and DMNCs is due to the removal of organic moieties on the surface, in addition to their structural transformation. The observed total weight loss of 11.2% in DMNCs is lower than that of the PAMAM dendrimer-functionalized systems,[21] due to the low surface areas of the nanosized magnetic particles. Thus, the TGA analyses indicate the coating of the organic moiety on the surface of the magnetite nanoparticles.

Fig. 5 shows a TEM micrograph (the inset shows the particle size distribution), and it can be seen that the nanoparticles are close to spherical and the particle sizes are in the range 5–15 nm with an average size of about 10 nm. This is in good agreement with the crystallite size of DMNCs obtained from XRD line broadening. However, a slight aggregation

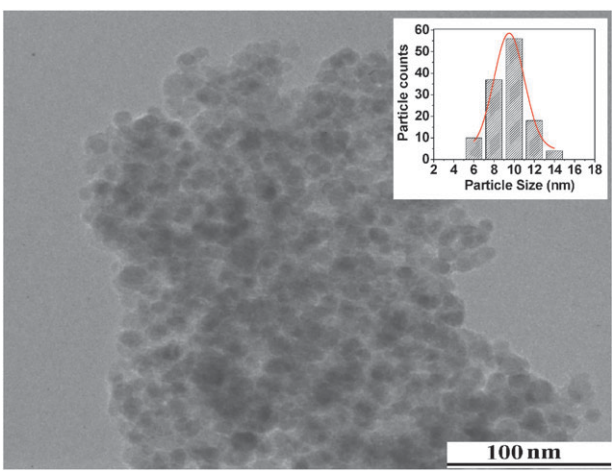

Fig. 5 TEM of the DMNCs (the inset shows the particle size distribution).

of nanoparticles is seen, possibly due to the presence of multilayers of particles on the TEM grid.

The particle size analysis of the MNPs and the DMNCs was also done by means of dynamic light scattering particle size analysis (DLS). The mean hydrodynamic diameters of MNPs, APTS-coated MNPs and DMNCs were found to be 147, 157 and 172 nm (σ < 10%), respectively. According to DLS experiments, the diameter of the MNPs increased marginally with the coating with APTS, but a marked increase was observed with the attachment of the dendritic block. The observed increase in mean hydrodynamic diameter of APTS-coated MNPs and DMNCs is mainly due to the presence of associated and hydrated organic layers on the surface of MNPs. In addition to the above, the clustering of nanoparticles may also influence the hydrodynamic diameter of the system in solution. Furthermore, the results indicate that the Fe_3O_4 (MNP) particles have been successfully functionalized with APTS and a dendritic shell.

Fig. 6 shows field-dependent magnetization curves of MNPs, APTS-coated MNPs and DMNCs. The magnetization curves exhibit zero remanence and zero coercivity, which proves that MNPs, APTS-coated MNPs and DMNCs are single-domain particles with superparamagnetic properties.[22] The maximum magnetization at 2 T were found to be 67.3, 63.2 and 48.4 emu g^{-1} for MNP, APTS-coated MNP and DMNCs, respectively. The magnetization of DMNCs reduces by 25–30% compared to MNPs, whereas TGA shows reduction of only 8.2%. The magnetization of MNPs is possibly associated with the clustering behavior of the bare MNPs which, in turn, increases the net magnetic moment due to exchange coupling and dipolar interactions among the surface ions.[23] The observable decrease of magnetization for the DMNCs was mainly due to the presence of a larger amount of non-magnetic dendritic blocks on the surface of the MNPs, which also suppresses the exchange coupling and dipolar interactions among coated nanoparticles. These results further support the functionalization of magnetic nanoparticles.

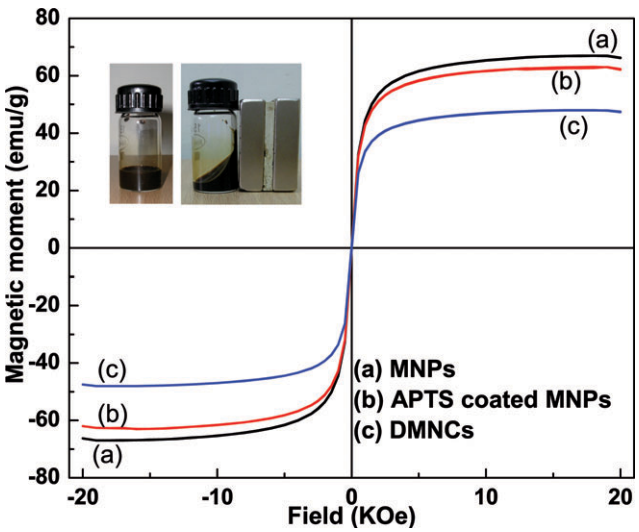

Fig. 6 Magnetization curves of the MNPs, APTS-coated MNPs and DMNC, and photographs showing well-dispersed DMNCs and the nanocarriers attracted towards a magnet.

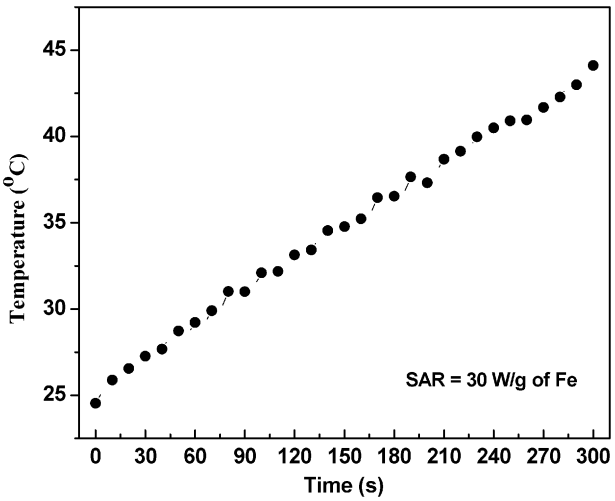

Fig. 7 Time-dependent temperature rise of DMNCs under an AC magnetic field.

Fig. 7 shows the time-dependent temperature rise of DMNCs under applied AC magnetic field of 10 kA m^{-1} and 425 kHz frequency. The specific absorption rate (SAR) was calculated from the initial slope of the time–temperature curve of different concentrations of the sample and was found to be 30 W g^{-1}. However, the SAR value is dependent on several parameters, such as the magnitude of the AC magnetic field (H), frequency (ω) and physical properties of magnetic particles such as magnetization and particle size. In the range of superparamagnetic particle size, the SAR depends linearly on the frequency and follows a square law with the AC field amplitude (H).[24] In practice, however, the heating efficiency of available particles cannot be raised simply by increasing the AC field amplitude and frequency, since in this way inductive heating of the healthy tissue would grow prohibitively high. Therefore, one can optimize the SAR value by varying the frequency, field and physical properties. In this work, the SAR value should not be viewed in terms of performance, but only as the demonstration that the nanocarriers are an effective heating source for possible hyperthermia treatment of cancer. The heating of superparamagnetic nanocarriers in an external alternating magnetic field is due to the rotation loss processes, which include Néel and Brownian relaxation loss.[25,26]

2.1 Biocompatibility of the developed system

The SRB assay showed that about 95 ± 3% of the cells were viable, even after incubation with 1 mg ml^{-1} of DMNCs (Fig. 8a). Furthermore, no significant cell death and change in cell morphology was observed on microscopic examinations of cells during the period of study (Fig. 8b). These results indicate that the viability of the HeLa cells is not affected by the presence of DMNCs, suggesting that nanocarriers are reasonably biocompatible and do not have toxic effects for further *in vivo* use.

2.2 *In vitro* drug loading and release

The average drug loading observed for the DMNCs was 64 ± 1.5% irrespective of the particle:drug ratio (8 : 1, 4 : 1,

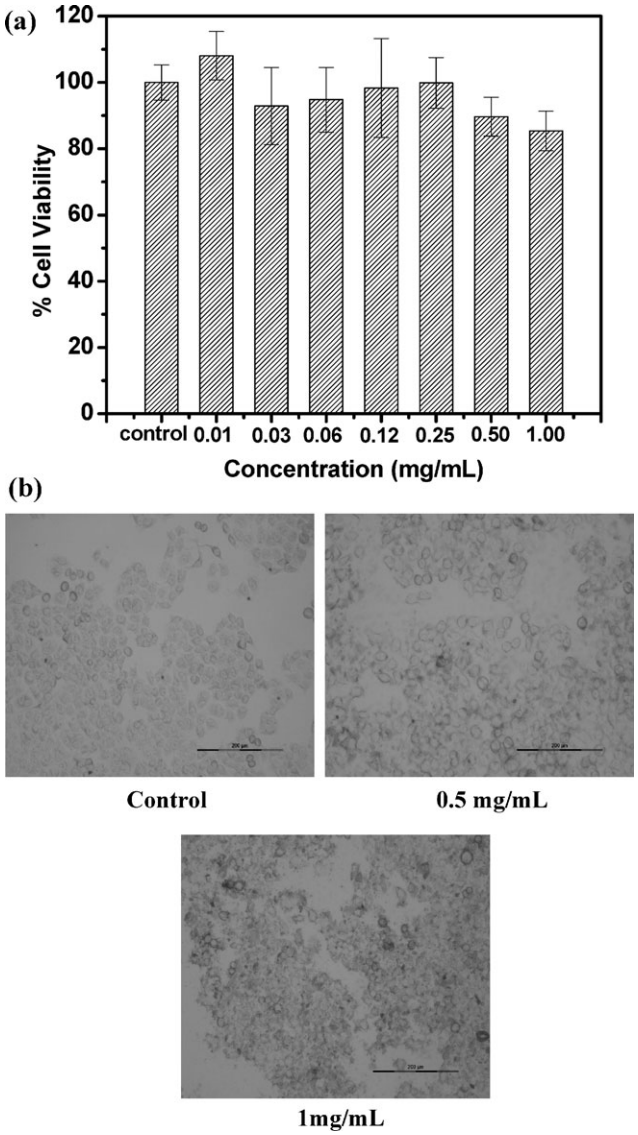

Fig. 8 (a) Viabilities of HeLa cells incubated with medium containing DMNCs. (b) Optical microscopy images of HeLa cells cultured with control (no DMNCs), 0.5 mg ml^{-1} DMNCs and 1 mg ml^{-1} DMNCs (scale bar is 200 μm).

2 : 1 and 1 : 1). Also, the particle:drug ratios show an increase in the drug loading capacity with time which slowly saturates, thereby accounting for the steric hindrances which interfere with the drug loading capacity of the dendritic nanocarrier. Fig. 9 shows the drug loading profile of doxorubicin (DOX) on to the magnetic nanocarriers. The fluorescence intensity is highly dependent on the state of the molecule, and hence can be used to determine whether the drug is free or in attached form. Thus, the observed decrease in fluorescence intensity confirmed the interactions between the drug molecules and DMNCs, thereby indicating the loading of the drug. Further, the zeta potential of the DMNCs (+17 mV) shifted to +2 mV due to the loading of the negatively charged DOX. The decrease in the zeta potential (15 mV) indicates that the drug molecules (DOX) were attached to the surface of DMNCs through the electrostatic interaction between positively

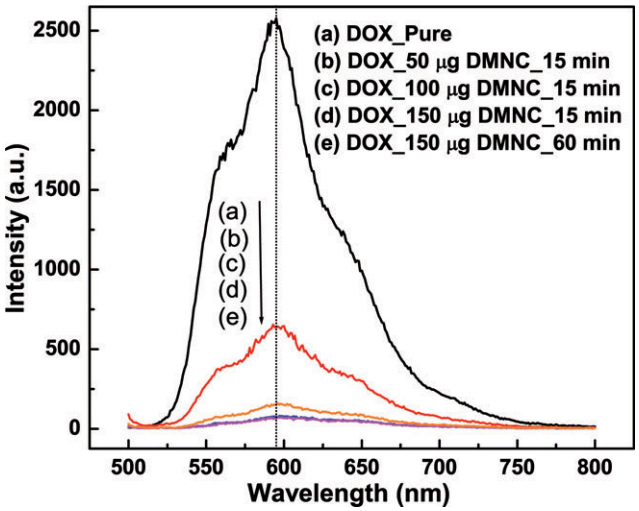

Fig. 9 Drug loading profile with a constant amount of DOX (10 μg mL^{-1}) using a variable amount of DMNCs (50–150 μg ml^{-1}) in milliQ water (pH 6) at room temperature.

charged DMNCs and negatively charged DOX, which shields the surface charge and shifts the shear plane to a larger distance.[27,28]

Fig. 10(a) shows the release profile for the DOX-loaded DMNCs (drug:particle = 1 : 4) as a function of time. The drug release profile clearly shows a sustained drug release over a period of 24 h, attaining a plateau after 8 h. Complete release of the drug was not observed, thereby giving the maximum release of 54%. Fig. 10(b) shows the drug release profiles of the DOX-loaded DMNCs in the absence and presence of the AC magnetic field. Initially, the increase follows a steady linear path which steepens upon application of the AC magnetic field. The increase in fluorescence can be attributed to the slow release of drug into the solution (inset Fig. 10(b)). About 35% of the drug was released in the first 45 min in the absence of a magnetic field. However, the release percentage further increased to ~80% under the continuous application of AC magnetic field over the next 15 min. As is evident, these preliminary results clearly indicate that in the presence of an AC magnetic field, the release of the drug molecule is enhanced, which is favorable for combined therapy involving drug delivery and hyperthermia.

Although techniques like TGA, DLS, XRD and VSM provide satisfactory evidence of the coating/functionalization of the magnetic nanoparticles; their structural elucidation still remains to be validated. Although FTIR provides evidence of the presence of the functional groups of the organic moieties, it does not clearly represent the structure. NMR could not be used to validate the structure, because the magnetic domains of our nanoparticles interfere with the signals. Hence, we do not rule out the possibility of the presence of biphasic suspension[29] (bare magnetic nanoparticles and the dendritic blocks) along with our DMNCs. In any case, our objective of the combined therapy is met, as the bare nanoparticles also participate in the heat generation and the unreacted dendritic blocks could efficiently carry and release the drug.

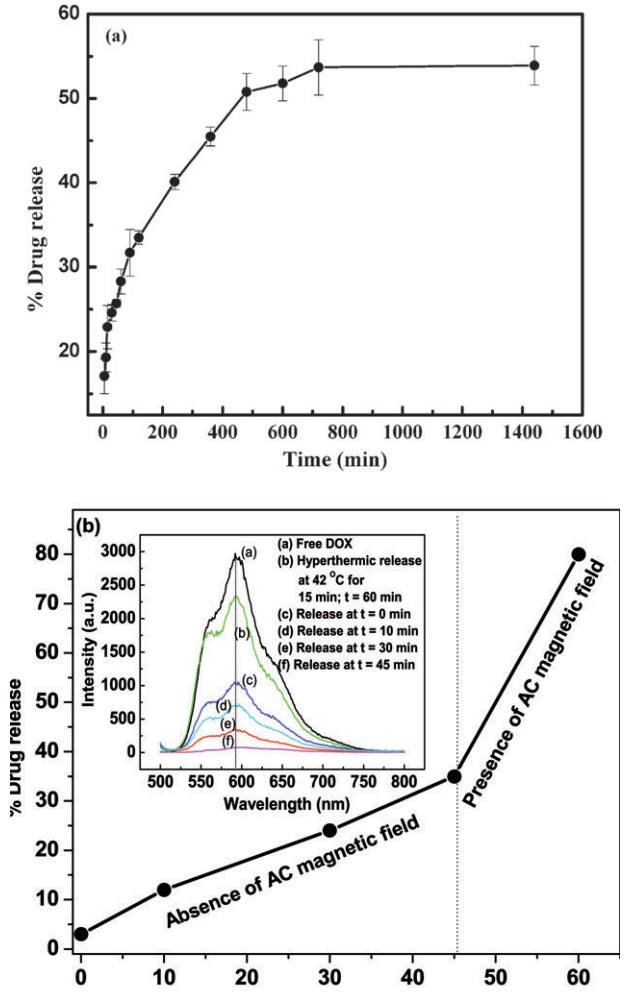

Fig. 10 (a) Drug release profile of DOX from the DMNCs in acetate buffer (pH 5) against PBS (pH 7.3) at room temperature. (b) Drug release (%) in the absence of an AC magnetic field (at room temperature) and presence of an AC magnetic field (at 42 °C) in acetate buffer (pH 5). Inset: Fluorescence spectra of the released drug from the DMNCs in absence and presence of AC magnetic field.

3. Experimental

3.1 Materials

Methyl acrylate and L-arginine monohydrate chloride were purchased from S.D. Fine Chem. Ltd. (India) and Spectrochem Pvt. Ltd. (India), respectively. Ferric chloride hexahydrate ($FeCl_3{\cdot}6H_2O$), ferrous chloride tetrahydrate ($FeCl_2{\cdot}4H_2O$) and 3-aminopropyltrimethoxysilane ($NH_2(CH_2)_3Si(OCH_3)_3$, APTS) were purchased from Sigma Aldrich . All chemicals were of analytical grade and were used as received.

3.2 Synthesis of dendritic magnetic nanocarriers (DMNCs)

3.2.1 Preparation of APTS-coated iron oxide magnetic nanoparticles. Magnetic nanoparticles (MNPs) were prepared by co-precipitation of Fe^{2+} and Fe^{3+} in the presence of NaOH.[30,31] Typically, a mixture of 25 ml of 1 M $FeCl_3{\cdot}6H_2O$, 25 ml of 0.5 M $FeCl_2{\cdot}4H_2O$ and 25 ml of 0.4 M HCl was stirred vigorously under N_2 in a 3-necked round-bottomed flask at 80 °C. 250 ml of NaOH (preheated to 80 °C) was then added. The black-coloured precipitates of MNPs were obtained by cooling the reaction mixture to room temperature and then rinsing with milliQ water five times. During each rinsing step, samples were separated from the supernatant using a permanent magnet (magnetic separation).

The above MNPs were then treated with APTS in an ultrasonic water bath for 30 min.[32] The resultant reaction mixture was rinsed with methanol and milliQ water five times by magnetic separation. The obtained APTS-coated magnetite nanoparticles were then dispersed in milliQ water using an ultrasonic water bath.

3.2.2 Growth of dendritic macromolecules on APTS-coated magnetic nanoparticles. Dendritic macromolecules were grown on the surface of APTS-coated magnetic nanoparticles by adding branched monomer of methyl acrylate, which reacted with the functional groups ($-NH_2$) of APTS.[28] The new end groups further reacted with a different monomer, arginine. In brief, 10 ml of methanol solution of APTS-coated iron oxide nanoparticles (0.5 g, 5 wt% mg ml^{-1}) was added to 20 ml of 20% (v/v) methyl acrylate methanol solution. The above mixture was sonicated in an ultrasonic water bath at room temperature for 7 h. The particles were then collected magnetically and rinsed with methanol five times by magnetic separation. After rinsing, arginine (15.5 g; 0.09 mol) was added and the suspension was again sonicated in an ultrasonic water bath at room temperature for 3 h. The particles were rinsed with methanol and separated magnetically. Thus, dendritic macromolecules were obtained which allows one to take advantage of its multivalency in creating functionalized exteriors with high ligand densities for drug loading.

3.3 Evaluation of specific absorption rate (SAR)

The heating ability of the DMNCs was measured from the time-dependent calorimetric measurements using a RF generator (Comdel CLF-5000).[33] 1 ml of magnetic suspension (10 mg ml^{-1} of Fe) was taken in a polypropylene sample holder with suitable arrangements to minimize the heat loss. The AC magnetic field of 10 kA m^{-1}, and a fixed frequency of 425 kHz was used to evaluate the SAR value. The SAR was calculated using the following equation:

$$\mathrm{SAR} = C\frac{\Delta T}{\Delta t}\frac{1}{m_{\mathrm{Fe}}}$$

where C is the specific heat of solvent ($C = C_{\mathrm{water}} = 4.18$ J g^{-1} K^{-1}), $\Delta T/\Delta t$ is the initial slope of the time-dependent temperature curve and m_{Fe} is the mass fraction of Fe in the sample.

3.4 Biocompatibility studies

The sulforhodamine-B (SRB) assay was performed to evaluate the biocompatibility of the DMNCs with HeLa cells. The cells were seeded into 96-well plates at densities of 1×10^5 cells per well for 24 h. Then DMNCs of 8 different Fe concentrations ranging from 0 to 1 mg ml^{-1} were added to the cells and incubated for 24 h at 37 °C and 5% CO_2. Thereafter, the cells were washed thrice with phosphate-buffered saline (PBS) and the cell viability determined with the SRB assay. For this, cells

were fixed with a solution of 25 μl of cold 50% trichloroacetic acid and stained with 0.4% SRB dissolved in 1% acetic acid. Cell-bound dye was extracted with 100 μl unbuffered Tris buffer solution (10 mM), and then the optical density (OD) was measured at 550 nm using a microplate spectrophotometer (Model 680, Bio-Rad, Japan). The experiment was performed in triplicate. The cell viability was calculated using the following formula:

$$\%\ \text{Cell viability} = \frac{\text{OD of treated cells}}{\text{OD of control cells}} \times 100$$

3.5 Drug loading and drug release studies

Doxorubicin (DOX) was used as a model anticancer agent. For incorporation of DOX into DMNCs, an aqueous solution of hydrochloride salt of DOX (2 mg ml^{-1}) was added to an aqueous dispersion of DMNCs (2 mg ml^{-1} of Fe). The solution was incubated for 1 h in the dark to load the drug on to the surface of magnetic nanocarriers. Drug-loaded nanocarriers were then separated from the free-standing drug using a permanent magnet and were washed thrice with milliQ water to remove the physically adsorbed drug molecules. The supernatant was analyzed at fixed wavelength (λ = 490 nm) using a Perkin Elmer 1420 multilabel counter to determine the percentage of drug loading against a standard plot which was prepared under identical conditions.

In order to investigate the interaction of drug molecules with DMNCs, we studied the fluorescence spectra of drug-loaded DMNCs. The aqueous dispersion of DMNCs (50, 100, 150 μg ml^{-1}) were added to the DOX solution (10 μg ml^{-1}) and incubated for 15–20 min in the dark to load DOX into DMNCs.

The drug release studies from drug-loaded DMNCs (particle:drug = 4 : 1; saturation loading point) were carried out under reservoir-sink conditions with 2 ml of acetate buffer (pH 5) against PBS (pH 7.3) as a sink at room temperature. After a definite interval of time, aliquots from the sink were extracted for analysis and an equal amount of medium added to the sink. DOX levels in the extracted samples were analyzed by measuring the fluorescence intensity at $\lambda_{excitation}$ = 490 nm and $\lambda_{emission}$ = 535 ± 30 nm against the standard plot prepared under similar conditions.

The drug release was also carried out in the presence of an AC magnetic field by utilizing the unique heating ability of the magnetic nanocarriers. The acetate buffer (pH 5) dispersion DOX-loaded DMNCs (taken in a polypropylene sample holder, with suitable arrangements to minimize the heat loss) was placed in an AC magnetic field. The magnetic field was initially increased to attain 42 °C (hyperthermia temperature) and this temperature was maintained for 15 min by varying the AC magnetic field.

3.6 Characterization techniques

X-ray diffraction (XRD) patterns were recorded on a powder X-ray diffractometer (Pananalytical) with Cu Kα radiation. The crystallite size was determined from the X-ray line broadening using the Scherrer formula:

$$D = 0.89\,\lambda/\beta\cos\theta,$$

where D is the average crystalline size, λ the X-ray wavelength used, β the angular line width at half maximum intensity and θ the Bragg angle. We have considered the instrumental error factors in calculation of crystallite size and lattice parameters. The infrared spectra (FTIR) was obtained in the range 4000–400 cm^{-1} on a Fourier transform infrared spectrometer (Jasco, FTIR 300E spectrometer) using the KBr pellet method. Transmission electron microscopy (Philips, CM 200) was used for the determination of particle size (at an operating voltage of 200 keV). The hydrodynamic diameters were determined by dynamic light scattering (DLS, BI-9000AT Brookhaven Instruments Corp.). The surface charges on samples (pH = 6.6 ± 0.4) were measured using a zeta plus zeta potential analyzer (Brookhaven Instruments) at 25 °C. The field-dependence magnetization measurements were carried out by a vibrating sample magnetometer (VSM, Model 7410, LakeShore) at room temperature. The thermogravimetric analysis (TGA) of samples were performed using SDT Q600 thermogravimetric analyzer (TA Instruments) under N_2 atmosphere in the temperature range 30–500 °C at a heating rate of 5 °C min^{-1}. The fluorescence intensities were measured on a Hitachi F2500 spectrophotometer.

Conclusions

Magnetic Fe_3O_4–dendritic nanocarriers (DMNCs) were synthesized and characterized by various techniques. TEM and XRD analysis indicated that nanoparticles were close to spherical with an average particle size of 10 nm. The nanocarriers were superparamagnetic, and the magnetization in a field of 2 T was 48.4 emu g^{-1}. An optimum SAR of 30 W g^{-1} of Fe was observed for the nanocarriers, which suggests that they can be efficiently used as magnetic-field-assisted drug delivery systems as well as for magnetism-induced hyperthermia. The presence of dendritic blocks on the surface of the magnetic nanoparticles and their interaction with the drug is evident. The drug incorporation efficiency of doxorubicin in DMNCs was found to be 65% with sustained release of 54% over a period of 8 h. Although the results of biocompatibility are preliminary, and more extensive toxicity studies in animal models are required to ascertain their usefulness and safety *in vivo*, they are satisfactory enough to allow further studies into the use of such suspensions for possible combined therapy. This study opens up several possibilities of using biphasic suspensions with multifunctional capabilities, along with enhanced drug delivery under high frequency AC magnetic field.

Acknowledgements

SC gratefully acknowledges the Department of Science and Technology, Govt. of India, for awarding a Fast Track Young Scientist fellowship. A financial grant from Nanomission DST is also gratefully acknowledged.

References

1 L. M. Rossi, A. D. Quach and Z. Rosenzweig, *Anal. Bioanal. Chem.*, 2004, **380**, 606–613.
2 M. Gao, L. Li, P.-L. Ho, G. C. Mak, H. Gu and B. Xu, *Adv. Mater.*, 2006, **18**, 3145–3148.

3 S. Mornet, S. Vasseur, F. Grasset, P. Verveka, G. Goglio, A. Demourgues, J. Portier, E. Pollert and E. Duguet, *Prog. Solid State Chem.*, 2006, **34**, 237–247.
4 A. K. Gupta and M. Gupta, *Biomaterials*, 2005, **26**, 3995–4021.
5 D. Bahadur and J. Giri, *Sadhana*, 2003, **28**, 639–656.
6 A. H. Lu, E. L. Salabas and F. Schüth, *Angew. Chem., Int. Ed.*, 2007, **46**, 1222–1244.
7 J. F. G. A. Jansen, E. M. M. de Brabander-van den Berg and E. W. Meijer, *Science*, 1994, **266**, 1226–1229.
8 G. R. Newkome, B. D. Woosley, E. He, C. N. Moorefield, R. Güther, G. R. Baker, G. H. Escamilla, J. Merrill and H. J. Luftmann, *Chem. Commun.*, 1996, 2737–2738.
9 C. Liu, C. Gao and D. Yan, *Macromolecules*, 2006, **39**, 8102–8111.
10 C. M. Paleos, D. Tsiourvas, Z. Sideratou and L. Tziveleka, *Biomacromolecules*, 2004, **5**, 524–529.
11 J. Lim and E. E. Simanek, *Mol. Pharmaceutics*, 2005, **2**, 273–277.
12 F. M. H. de Groot, C. Albrecht, R. Koekkoek, P. H. Beusker and H. W. Scheeren, *Angew. Chem., Int. Ed.*, 2003, **42**, 4490–4493.
13 R. J. Amir, N. Pessah, M. Shamis and D. Shabat, *Angew. Chem., Int. Ed.*, 2003, **42**, 4494–4499.
14 R. S. Dhanikula and P. Hildgen, *Bioconjugate Chem.*, 2006, **17**, 29–41.
15 M. Sugimoto, T. Okagaki, S. Narisawa, Y. Koida and K. Nakajima, *Int. J. Pharm.*, 1998, **160**, 11–19.
16 N. Malik, R. Wiwattanapatapee, R. Klopsch, K. Lorenz, H. Frey, J. W. Weener, E. W. Meijer, W. Paulus and R. Duncan R, *J. Controlled Release*, 2000, **65**, 133–148.
17 S. Supattapone, H. Wille, L. Uyechi, J. Safar, P. Tremblay, F. C. Szoka Jr, F. E. Cohen, S. B. Prusiner and M. R. Scott, *J. Virol.*, 2001, **75**, 3453–3461.
18 R. Duncan and N. Malik, *Proc. Int. Symp. Control. Release Bioact. Mater.*, 1996, **23**, 105–106.
19 P. P. Albert, P. B. Michel and P. Chellapah, *Langmuir*, 1994, **10**, 92–99.
20 G. Cao, *Nanostructures and Nanomaterials: Synthesis, properties and applications*, Imperial College Press, 2004, ch. 2.
21 Y. J. Jiang and Q. M. Gao, *J. Am. Chem. Soc.*, 2006, **128**, 716–717.
22 M. A. Zhiya, G. Yueping and H. Liu, *J. Polym. Sci., Part A: Polym. Chem.*, 2005, **43**, 3433–3439.
23 K. C. Barick, M. Aslam, Y.-P. Lin, D. Bahadur, P. V. Prasad and V. P. Dravid, *J. Mater. Chem.*, 2009, **19**, 7023–7029.
24 R. Hergt, R. Hiergeist, M. Zeisberger, G. Glöckl, W. Weitschies, L. P. Ramirez, I. Hilger and W. A. Kaiser, *J. Magn. Magn. Mater.*, 2004, **280**, 358–368.
25 R. Hergt, W. Andrä, C. G. d'Ambly, I. Hilger, W. A. Kaiser, U. Richter and H. G. Schmidt, *IEEE Trans. Magn.*, 1998, **34**, 3745–3754.
26 N. K. Prasad, K. Rathinasamy, D. Panda and D. Bahadur, *J. Mater. Chem.*, 2007, **17**, 5042–5051.
27 R. Gref, A. Domb, P. Quellec, T. Blunk, R. H. Muller, J. M. Verbavatz and R. Langer, *Adv. Drug Delivery Rev.*, 1995, **16**, 215–233.
28 A. E. Hawley, L. Illum and S. S. Davis, *Pharm. Res.*, 1997, **14**, 657–661.
29 N. K. Prasad, L. Hardel, E. Duguet and D. Bahadur, *J. Magn. Magn. Mater.*, 2009, **321**, 1490–1492.
30 B. Pan, F. Gao and L. Ao L, *J. Magn. Magn. Mater.*, 2005, **293**, 252–258.
31 B. Pan, D. Cui, F. Gao and R. He, *Nanotechnology*, 2006, **17**, 2483–2489.
32 Y. Lu, Y. Yin, B. T. Mayers and Y. Xia Y, *Nano Lett.*, 2002, **2**, 183–186.
33 P. Pradhan, J. Giri, G. Samanta, H. D. Sarma, K. P. Mishra, J. Bellare, R. Banerjee and D. Bahadur, *J. Biomed. Mater. Res., Part B: Appl. Biomater.*, 2006, **81**, 12–22.